

**BISMUTH HALL THRUSTER II:
SIMULATED DIAGNOSTICS**

D. B. S C H A R F E, M. A. C A P P E L L I

Stanford University
Mechanical Engineering Department
Stanford, CA 94305 USA
e-mail: scharfe@stanford.edu

A laboratory-model bismuth-fueled Hall thruster has been designed, and the geometry of that design has been incorporated into a 2-D radial-axial hybrid Hall thruster simulation. Velocity distribution data from the plume of that simulation, incorporated with calculations based on the known spectroscopy of the bismuth ion, have been used to simulate optical diagnostic measurements of the exhaust velocity of the thruster. Simulated Laser Induced Fluorescence and emission spectroscopy data has been produced, assuming that the 14681.971 cm^{-1} transition of ionized bismuth is analyzed. The simulated Laser Induced Fluorescence assumes a narrow line-width, scanning laser probes the plasma either axially or radially, and it is suggested that the fluorescence be collected about the 15146.544 cm^{-1} transition; emission results have been simulated with varying instrument resolutions and with collection angles at 0° and 60° off the axial axis.

1. Introduction

Within the scientific community, there is much interest in exploring the environments of the outer planets of the solar system via unmanned probes. High-powered electric propulsion (E.P.) systems, consuming hundreds of kilowatts, have been suggested to achieve a fast mission to the outer planets [5].

Nuclear power systems have been proposed to provide the required 10's to 100's of kilowatts of required power to the spacecraft, but state-of-the-art E.P. systems are generally capable of handling only about 10 kW of power [5]. Therefore, several advanced technologies have been proposed to develop electric propulsion systems with increased power-handling capabilities. One proposal, a Very High Power Thruster with Anode Layer (later termed Very High I_{sp} Thruster with Anode Layer, or VHITAL [11]) centers around the adaptation of a Russian-developed Hall thruster utilizing bismuth as a propellant [18]. The proposed thruster builds on a Russian design which has already been demonstrated to run at 140 kW and should be scalable to even higher power levels. Further, the VHITAL design would use a two-stage mechanism to accelerate the exhaust gas to 70 km/s; such a high exhaust velocity provides for a very efficient use of propellant. Adding additional efficiency to the system, the proposed bismuth propellant has a low 7.3 eV ionization energy and a high atomic mass of 209 amu. Such a thruster is expected to provide the power-handling and efficiency required to make

a Nuclear Electric Propulsion (N.E.P.) mission to the outer planets feasible in the near future.

As any new thruster is developed, it is necessary to characterize its performance so that the thruster, and the system in which it will be integrated, can be fully understood and optimized. In order to optimize a bismuth-fed thruster, it will be necessary to run a suite of diagnostics, perhaps the most important of which will be a non-intrusive optical measurement to determine the velocity distribution of the ions in the thruster plume. However, without the yet-to-be completed VHITAL thruster in hand, the development of this diagnostic will be contingent on theoretical work, simulations, and experimentation with simpler laboratory-model thrusters.

In the first paper of this series, titled Bismuth Hall Thruster I: Simulation-suggested Design and Performance, the prototype thruster design was described, and general simulation results of thruster performance with various channel lengths were presented. In this paper, the theoretical work and transition selection for velocity measurement of the bismuth ion (Bi II) in a physical thruster will be discussed. Simulated ion velocity distribution data for this thruster, produced by 2-D radial-axial hybrid Hall thruster simulation running bismuth propellant, will be presented. The simulated velocity distributions will then be utilized in producing likely Laser Induced Fluorescence (LIF) and emission spectroscopy data to predict probable experimental results from the laboratory model thruster and provide some insight into the potential accuracy of a variety of measurements.

2. Bismuth Spectroscopy

2.1. Transition selection. When selecting a transition for emission measurements of the bismuth ions, the relative strength of the transition and the convenience of the particular wavelength are the primary selection criteria. Candidate transitions for velocity determination via LIF analysis of ions were chosen based, in part, on accessibility to commercially available diode laser systems for simplicity. Specifically, the New Focus TLB-6309, which can scan 680–690 nm, has been selected to probe the Bi II transition listed at 680.86 nm according to the U.S. National Institute of Standards and Technology (NIST) based on the 1934 work of CRAWFORD and MCLAY [3]. The 2002 work of DOLK, *et al.* place this line at 680.92 nm in air, with designation $6p7s (1/2,1/2)_1 - 6p7p (1/2,1/2)_1$, and center-of-gravity vacuum wavenumber $14681.971 \text{ cm}^{-1}$ [4]. This corresponds to a vacuum wavelength of 681.11 nm.

The selection of the $14681.971 \text{ cm}^{-1}$ transition, for both emission and LIF measurements, provides several advantages. Aside from being accessible to a suitable laser, the 681.1 nm line is a relatively strong transition [3, 4]; in fact, it is the strongest Bi II line in the 600–900 nm region that is most convenient for this work, which should help to maximize the signal in emission and LIF measurements. Additionally, an analysis of the energy level structure of Bi II, depicted in Fig. 1, shows that the 681.1 nm transition shares an upper state with the 660.2 nm transition (660.03 nm in air [4]), which may be useful for non-resonant LIF collection. The 660.2 nm transition (configuration: $6p7s (1/2,1/2)_0 - 6p7p (1/2,1/2)_1$, $15146.554 \text{ cm}^{-1}$) is the second strongest Bi II line in the region of interest [3, 4]. High intensity of both the probed transition and the collected transition should help to maximize signal strength in thruster measurements.

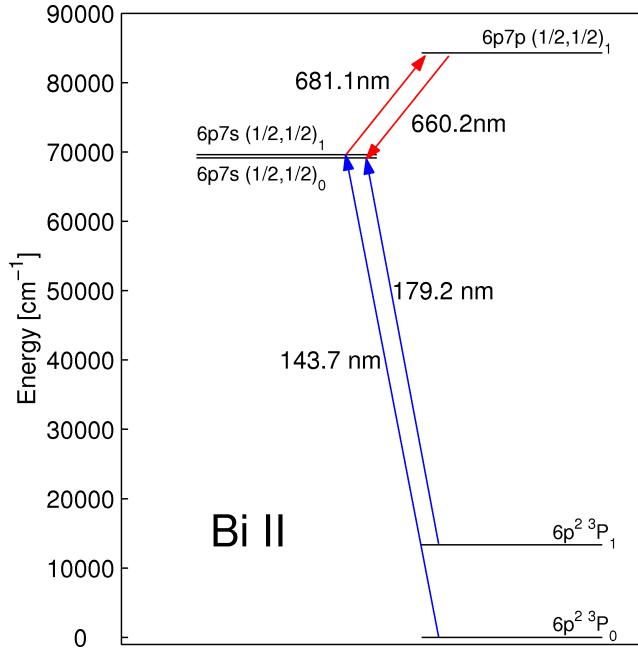


FIG. 1. Partial energy level diagram of Bi II indicating transitions of interest. Wavelengths as measured in vacuum.

Further, DOLK *et al.* state that the “connection between the two lowest levels...of the ground configuration [of Bi II] and the excited configurations is established by the lines at 1436 Angstroms and 1791 Angstroms” [4]. A further analysis of the energy level structure of Bi II, also illustrated in Fig. 1, shows that these ultra-violet transitions, which provide a bottleneck for the excitation and de-excitation of Bi II states, connect the ground configurations of Bi II with the lower levels of the 681.1 nm and 660.2 nm transitions. Therefore, the lower level of the 681.1 nm transition should be well populated, further maximizing the number of ions that can be excited by a laser at this wavelength and improving the potential for LIF signal strength.

2.2. Detailed spectroscopy. When transitions between electronic energy levels occur in a given atom, the energy absorbed or released by the atom is often accounted for by the absorption or emission of a photon; this interaction is a key to the spectroscopic study herein engaged. The photon energy, by way of its wavelength, λ , must equal the difference in energy, ΔE , between the starting and ending electronic states of the transition according to:

$$(2.1) \quad \lambda = \frac{hc}{\Delta E}.$$

Here, h is Planck’s constant and c is the speed of light in vacuum. Therefore, the wavelength derived via this equation would be that measured in vacuum.

When measured with high resolution, however, an electronic transition shows additional structure due to the effects of different isotopes in the gas as well as interactions between the electron cloud and the nuclear spin of the atom. This effect is termed hyperfine splitting. Bismuth 209 is the only stable isotope of bismuth found in nature, so the effects of isotopic splitting need not be discussed here. The nuclear spin splitting comes about because the nucleus of an atom or ion possesses an intrinsic angular momentum with an associated magnetic moment and nuclear spin quantum number, I . The orientation of the nuclear spin vector relative to the total angular momentum held in the electrons, J , creates another path by which energy levels can be split. This splitting is calculated by using an additional quantum number, F , which represents the vector sum of the electronic and nuclear angular momentums. As the vectors may have various different orientations relative to each other, F can take on multiple values according to [9]:

$$(2.2) \quad F = J + I, J + I - 1, \dots, |J - I|.$$

It should be noted, however, that for elements with a high nuclear spin, J is typically smaller than I so that the total number of F values is limited to $2J + 1$.

For convenience, another variable, C , is defined for each F value:

$$(2.3) \quad C = F(F + 1) - I(I + 1) - J(J + 1)$$

and each F value creates a shift from a given electronic energy level according to:

$$(2.4) \quad \delta E = \frac{1}{2}AC + B \frac{3C(C + 1) - 4I(I + 1)J(J + 1)}{8I(2I - 1)J(2J - 1)},$$

where A and B are hyperfine splitting parameters for a given electronic state and relate to the magnetic moment and the interaction of the quadrupole moment with the electron shell, respectively [2, 4, 9, 17].

The various δE values for the upper and lower states of a given electronic transition can be calculated via Eq. (2.4), splitting each state into multiple closely spaced energy levels with different F values. The subsequent transitions between the split energy levels of the upper and lower states, effectively having energy differences equal to the original ΔE altered by one or more δE values, must follow the selection rule:

$$(2.5) \quad \Delta F = 0, \pm 1,$$

but with transitions between two $F = 0$ states being forbidden.

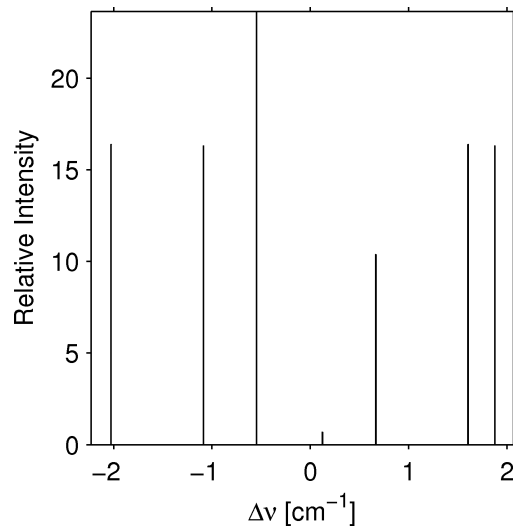
Calculations using the above equations and selection rules for transitions between the split states of an upper and lower electronic energy level will give the discrete wavelengths (or frequencies) of the corresponding hyperfine split transition. The relative intensities of the lines for a given hyperfine split transition are calculated from the sum rules [2, 17], which translate to the formulas defined by KUHN [10].

The nuclear spin quantum number for bismuth is $I = 9/2$ [4]. In the $14681.971 \text{ cm}^{-1}$ transition of Bi II, the splitting constants are $A = 390.7 \text{ mK}$, $B = 3 \text{ mK}$ for the lower state and $A = 269.25 \text{ mK}$, $B = 1 \text{ mK}$ for the upper state (note that $1 \text{ mK} = 10^{-3} \text{ cm}^{-1}$) [4].

Combining all of the above, the calculated hyperfine structure for the 681.1 nm ($14681.971 \text{ cm}^{-1}$) transition of Bi II is provided in Table 1 and shown in Fig. 2. The

Table 1. Calculated hyperfine splitting structure of Bi II line centered at $14681.971 \text{ cm}^{-1}$.

Shift [cm^{-1}]	Rel. Intensity
-2.0288	16.3636
-1.0877	16.2963
-0.5470	23.6364
0.1228	0.6734
0.6671	10.3704
1.6046	16.3636
1.8776	16.2963

FIG. 2. Hyperfine splitting of 681.1 nm transition of Bi II, relative to the center of gravity frequency of the transition, $14681.971 \text{ cm}^{-1}$.

absolute amplitudes of the hyperfine peaks illustrated here are somewhat arbitrary, with the sum of all amplitudes set to 100; the relative amplitudes, however, are calculated from KUNN's method [10]. The hyperfine split transition is shown again in Fig. 3 in vacuum wavelength space. Note that the hyperfine split transition is roughly 4 cm^{-1} across in wavenumber space, or 0.2 nm wide when measured in wavelength units. The strong coupling between the nucleus and the electrons in bismuth produce a hyperfine splitting that is an order of magnitude wider than that observed for the transitions typically analyzed in a xenon Hall thruster [2].

Going a step further in the spectroscopy-based analysis, in a physical system, transitions are broadened into continuous profiles. This broadening can come from a variety of effects, but we are primarily interested in that due to the motion of the atoms.

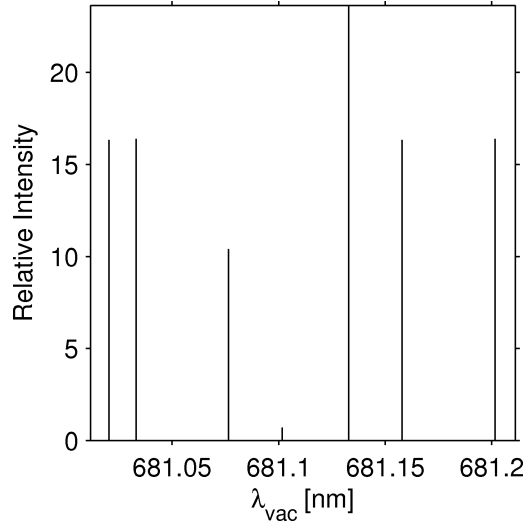


FIG. 3. Hyperfine splitting of 681.1 nm transition of Bi II in units of wavelength.

Specifically, velocimetry requires a measurement of the Doppler shift:

$$(2.6) \quad \delta\nu = \nu_0 \frac{u}{c},$$

where ν_0 is the unshifted frequency, u is the component of the velocity of a particle along the direction of light interaction, c is the speed of light, and $\delta\nu$ is an apparent frequency shift. For LIF analysis, the measurement entails a determination of the Doppler shift of the incoming laser light relative to the plume ions; in emission, the Doppler shift is the result of ions moving relative to the collection optics. When a group of particles all have different velocities, the result is a measurement of a continuum of frequency or wavelength shifts with respect to the expected unshifted values.

3. Simulated Velocity Distributions

In order to predict the likely velocity distribution, a Hall thruster simulation has been modified to model an in-development, laboratory-model, bismuth Hall thruster. The simulated thruster is a modification of the xenon-fueled Stanford Hall Thruster described by HARGUS [8] and MEEZAN [12]. As described by SCHARFE, *et al.*, and in the first paper of this series, the thruster has been modified with a secondary anode that doubles as a bismuth vaporizer and is placed a few centimeters from the end of the channel [13]. As suggested by the simulation of this thruster described in Part I of this series, the optimum channel length for bismuth operation was found to be 2.4 cm. Aside from the shortening of the channel and the switch to bismuth propellant, other aspects of the Stanford Hall Thruster remain unchanged in both the simulation and the laboratory thruster: it is a coaxial Hall-effect thruster characterized by an annular channel 1.2 cm wide with an inner radius of 3.5 cm. The simulation itself calculates particle motions

in a 2-dimensional radial-axial slice of the Hall thruster channel and a section of the near-field plume region. Heavy particles (ions and neutrals) are modeled as discrete superparticles; electrons are treated as a one-dimensional fluid. Specific details of the numerical model used have been discussed by M. SCHARFE, *et al.* [14, 15]; for the bismuth simulations discussed here, the shear-based electron mobility model has been used [14, 16]. For the bismuth thruster simulation, the code was run with a 200 V anode potential, 3.18 mg/s bismuth mass-flow rate, and with shear model coefficients $C = 16 \times 10^{-8}$ s, $\omega\tau_{\text{fluc}} = 8$, and $\alpha = 2$.

Running the simulation under these conditions, and with the simulation-optimized channel length of 2.4 cm, ion velocity distribution data were collected along the centerline of the 2-D simulated channel. The radial and axial velocity distributions at the thruster exit plane and in the plume, 4 cm downstream of the exit, are shown in Fig. 4. The velocity distributions have been smoothed to reduce statistical noise, generated by the PIC formulation of the plasma density, and normalized to integrate to unity. Since the velocity distribution data at each location is computed using exactly the same particles, the magnitudes of the radial and axial distributions at a given physical position can be compared.

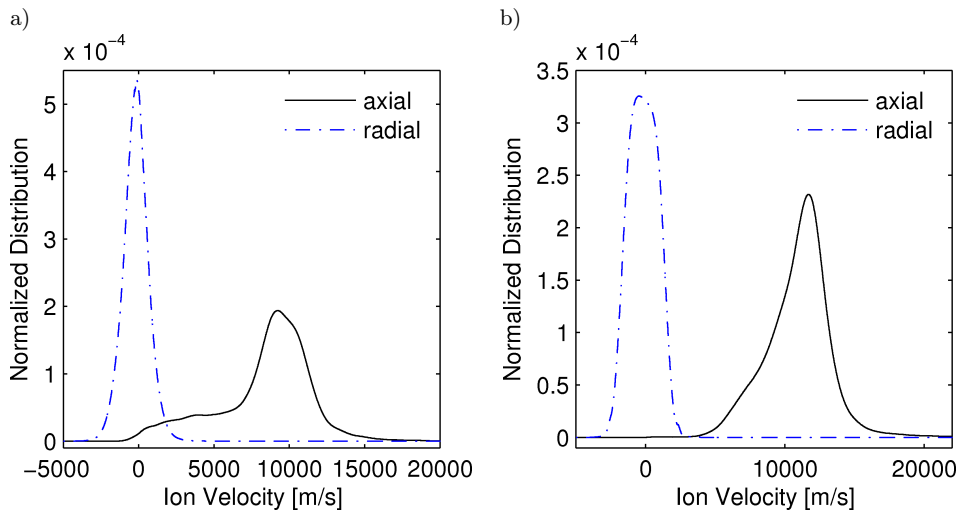


FIG. 4. Simulated radial and axial ion velocity distributions along the thruster centerline at: a) the thruster exit plane and b) in the plume near the edge of the grid domain, 4 cm from the exit plane.

4. Simulated LIF

When an electronic transition in a plasma is interrogated via Laser Induced Fluorescence, the incoming laser beam is typically projected antiparallel to the direction of bulk motion (especially for obtaining axial velocity data from a Hall thruster). In this case, particles moving toward the incoming laser light interact with light that is Doppler shifted toward a higher frequency. As a result, the particles become excited when the laser is at a lower frequency, or higher wavelength, than the unshifted transition frequency.

Figure 5 indicates the simulated LIF results for the Stanford Hall Thruster converted to run with bismuth propellant. It is assumed here that the laser linewidth is suitably narrow so as not to add uncertainty to the measurement. Simulated data indicates the fluorescence measurements that would be recorded as a result of laser excitation projected along the radial and axial directions. The data presented here is based on the simulated velocity distributions at the thruster exit plane on the channel centerline. Note that the radial velocity distribution is roughly symmetric about zero; this data could, theoretically, be used to pinpoint the unshifted hyperfine peak locations, and therefore interpret the velocity distribution from the axial LIF profile. One could also use some other stationary line source as a wavelength/frequency reference for measuring the shifted transition frequency. If one has confidence in the absolute frequency measurement of the laser beam, however, a simple comparison between the recorded LIF profile and the expected hyperfine profile, as illustrated in Fig. 3, may also suffice.

While the absolute magnitudes of the profiles in Fig. 5 are effectively arbitrary, the relative strengths of the radial and axial profiles can be compared; the radial profile shows a stronger signal since particle velocities in the radial direction are more tightly packed while those in the axial direction have a more significant spread.

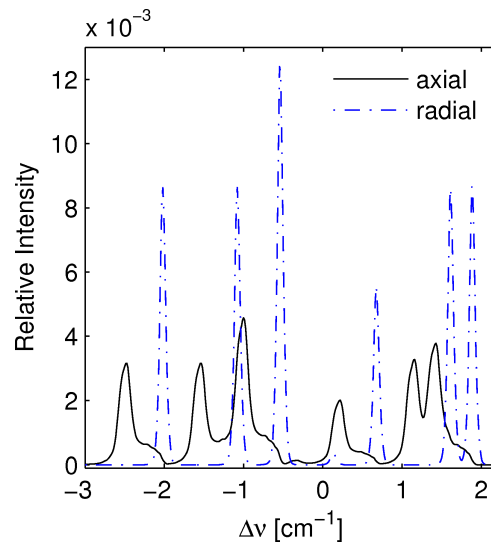


FIG. 5. Simulated radial and axial LIF data of the $14681.971 \text{ cm}^{-1}$ line of Bi II at the thruster exit plane. The x -axis indicates laser detuning relative to the transition center of gravity wavenumber.

Also of interest in Fig. 5 is the fact that, even with the velocity-broadened profile considered, the hyperfine structure can be resolved. This is quite unlike the nature of xenon, for which the hyperfine structure is much narrower and is entirely obscured by a typical Hall thruster velocity distribution [2]. This fact presents an opportunity to more easily estimate the velocity distribution function of a bismuth thruster since the broadened hyperfine peaks of bismuth do not significantly interfere with each other. Simultaneously, however, the width of this profile adds an additional difficulty: the broad hyperfine splitting effectively spreads the ions out over a wider range of frequency or

wavelength space, effectively reducing the signal strength available for measurement within a small range therein.

5. Simulated Emission

In emission spectroscopy, the Doppler shift is defined by the velocity of the plasma particles relative to the collection optics. In this case, light emitted from an ion that is moving toward the collection optics appears at a higher frequency than the theoretical value for the transition in question. In emission, therefore, when collection optics are placed downstream of the thruster, the axial velocity of ions in the Hall thruster plume will cause a shift toward higher frequency or lower wavelength.

Emission measurement also suffers from certain limits which may be avoided using an easily-directed narrow-linewidth laser as in LIF studies. Collection of emission data generally requires an instrument with finite resolving power; this may range from the picometer scale of the interferometer used by GAWRON, *et al.* in analyzing a xenon Hall thruster [7] up to the hundredths or tenths of a nanometer resolution that may be achievable by monochromators of various sizes. Additionally, emission measurements typically require the use of fairly large optics for gathering signal, and facility limitations may not allow placement of those optics perfectly along the axial or radial directions of a thruster. The location of the optics defines the angle at which the Doppler shift is observed, so collection at an angle off the thruster axis, like that performed by GAWRON, *et al.* [7], can also influence the observed results. This section will attempt to provide some insight into velocimetry via emission spectroscopy.

Of additional note is that emission measurements are typically made in the wavelength domain. Defining wavelength absolutely requires well calibrated instruments, and measurements made in air can still vary somewhat with local conditions such as humidity [1, 6]. Therefore, for absolute clarity, the wavelengths provided in this section are the vacuum wavelength values, which can be directly calculated from transition frequency.

5.1. Instrument resolution. Instrument resolution plays a strong role in determining exactly what information can be gleaned from measurements of emission from a Hall thruster. Figure 6 simulates emission data collected with various instrument resolutions. Beginning with a pure emission profile, the simulated instrument measurement was produced by effectively integrating the signal present within $\pm 1/2$ of the resolution about a given central wavelength. Effectively, this assumes a top-hat profile for instrument acceptance as a function of wavelength. Note, additionally, that with decreasing resolution (i.e.: wider range of wavelength acceptance) comes a larger signal; it is assumed for illustrative purposes that instrument sensitivity is not adjusted with resolution. In this way, it is clear that widening the slits of a monochromator provides a larger signal amplitude as more light is collected; simultaneously, however, the observable detail decreases.

As illustrated in plot (a) of Fig. 6, with instrument resolution at 1 pm, similar to the 0.7 pm resolution achieved by GAWRON, *et al.* [7], a fairly precise measurement of the Bi II lineshape can be recorded. A comparison between the broadened but relatively unshifted radial emission and the shifted emission collected axially would allow one to measure the bulk velocity, and an analysis of the shape of each of the hyperfine peaks would provide an accurate measurement of the velocity distribution. With instrument

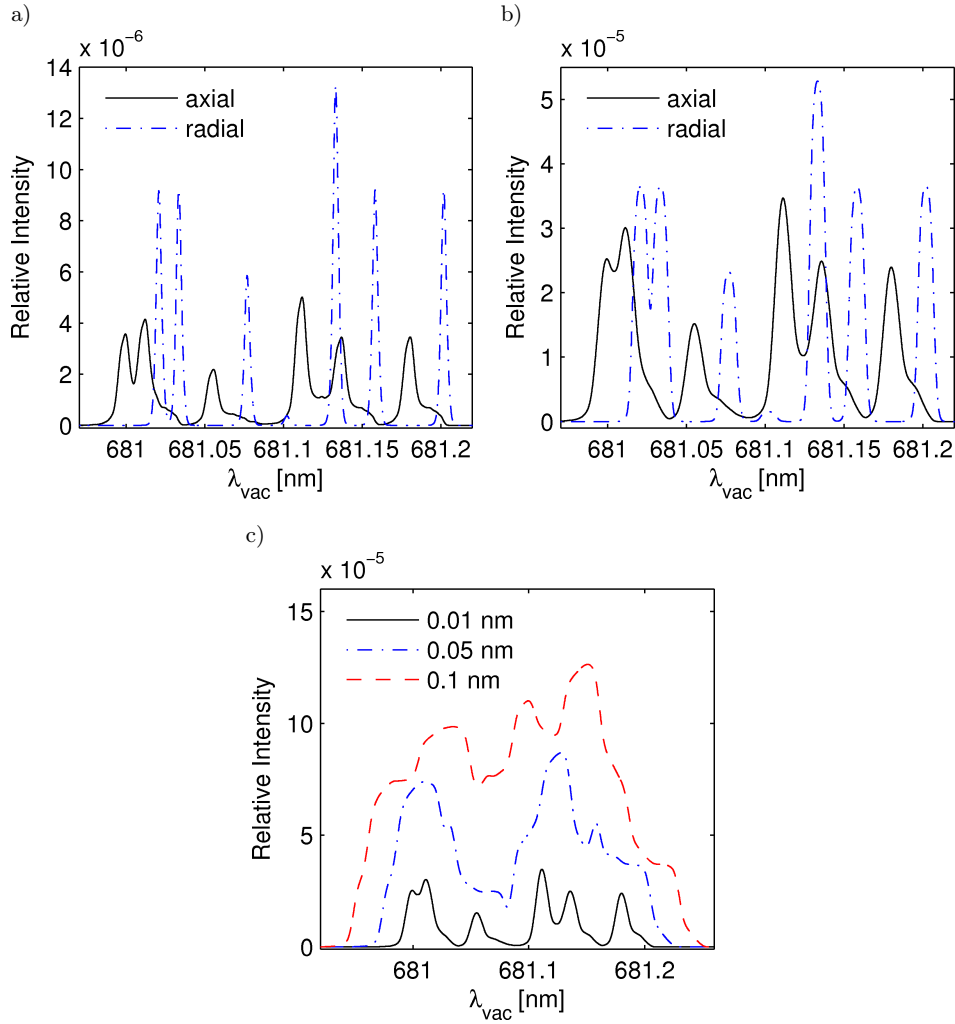


FIG. 6. Simulated emission data of the 681.1 nm Bi II transition at various instrument resolutions:
 a) simulated radial and axial emission collected with 1 pm resolution,
 b) radial and axial emission collected with 0.01 nm resolution, c) axial collection with resolutions indicated in the plot legend.

resolutions in the 0.01 nm range that might be achievable via a 1-meter focal length monochromator with relatively narrow slits, not much information is lost, as can be seen in plot (b) of Fig. 6. The troughs between the hyperfine peaks of the transition become relatively shallow by comparison to those in the higher resolution case, but the location of each peak is distinct and relatively unchanged; a reasonably accurate bulk velocity could certainly be measured relative to the unshifted radial emission, and it may also be possible to extract an approximate velocity distribution if one could account for the precise profile of instrument acceptance.

At the worse resolutions presented in plot (c) of Fig. 6, however, the underlying emission lineshape becomes less resolvable and the task of measuring velocity or velocity distribution becomes significantly less tractable. Note, again, that a simple top-hat profile was used in simulating instrument resolution here; an interpretation of experimental results would require a precise measurement of the actual instrument response for use in deconvolution calculations.

5.2. Off-axis collection. The positioning of collection optics also presents an issue for emission measurements. Effectively, measurements in emission record the velocity distribution of particles along the line-of-sight of those optics. As an illustration of this effect, simulated velocity distributions at various angles relative to the axial direction are shown in Fig. 7. In this case, 0° represents measurement from the axial direction; 90° would represent radial collection of emission data. Note that as the angle increases, the velocity distribution compresses and shifts towards zero, effectively approaching a radial velocity distribution. Collection at larger angles, therefore, will reduce the sensitivity to axial velocity. Note that GAWRON, *et al.* [7] collected at an angle of 59° .

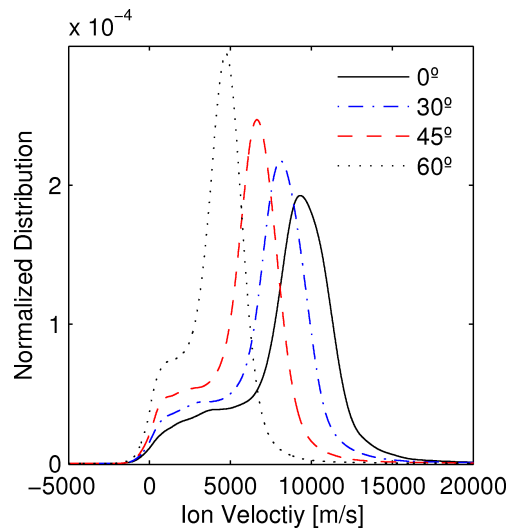


FIG. 7. Simulated velocity distributions at various angles measured off the axial axis of the thruster; recorded at the thruster exit plane along the thruster channel centerline.

Taking this a step further, simulated emission profiles, neglecting the effects of instrument resolution, are presented in Fig. 8, assuming collection at 0° and 60° relative to the thruster axis. Again, the simulation data used is that along the thruster channel centerline, at the exit plane. Note that, as expected, the profile at 60° appears relatively unshifted compared to that at 0° . It should be noted, however, that determining the axial velocity from a measurement taken at an angle is not necessarily a direct calculation; it is impossible to determine from a single emission measurement if the recorded Doppler shift is due to a velocity vector directed along the axis of collection, for example, or if the shift is due to a small component of a larger, more purely axial velocity.

Indeed, GAWRON, *et al.* used a detailed model, including measurement of low-velocity ions, to extract the axial velocity from their Fabry-Pérot measurements of Hall thruster emission [7].

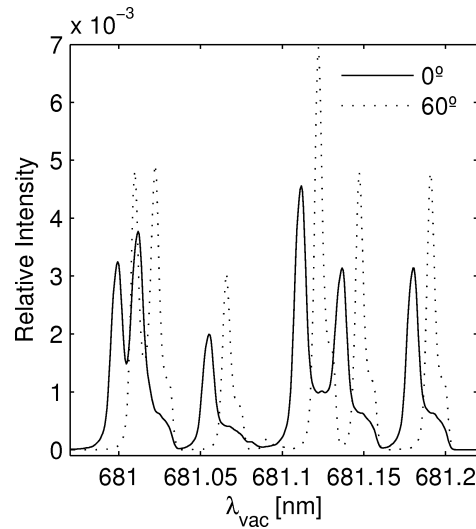


FIG. 8. Simulated emission measurements recorded with very fine instrument resolution at the exit plane of the thruster, with optics located at 0° and 60° off the thruster axial direction.

6. Conclusion

It should be noted that the simulated results presented here represent a best-case scenario for actual experiments. In the above work, there is no simulation of system noise, of the effects of collection optics or laser power, or of the precise signal that may be available as the emission coefficients of Bi II transitions are unavailable in the literature. Additionally, it has been assumed that the collection optics will receive signal from a single point in space, when in fact there will be emitting plasma along the optical line of sight which will increase experimental uncertainty. Nonetheless, the simulated results are promising, indicating that LIF and even emission spectroscopy with resolution in the range of 0.01 nm or better, should be able to provide adequate measurements of the velocity distribution of a bismuth thruster. The width of the bismuth hyperfine spectrum, while creating the difficulty of a weaker, more spread-out signal, also provides the opportunity to more precisely resolve the velocity distribution function by analyzing the shape of a single hyperfine peak.

Acknowledgments

Work was performed under the Department of Defense's NDSEG fellowship and the National Science Foundation's Graduate Research Fellowship Program.

References

1. G. BÖNSCH, E. POTULSKI, *Measurement of the refractive index of air and comparison with modified Edlén's formulae*, *Metrologia*, **35**, 133–139, 1998.
2. R.J. CEDOLIN, *Laser-Induced Fluorescence Diagnostics of Xenon Plasmas*, Ph.D. Thesis, Leland Stanford Junior University, Stanford, California 1997.
3. M.F. CRAWFORD, A.B. MCLAY, *Spark spectra of Bismuth, Bi III, and Bi II*, *Proceedings of the Royal Society of London, Series A*, **143**, 850, 540–557, 1934.
4. L. DOLK, U. LITZÉN, G.M. WAHLGREN, *The laboratory analysis of Bi II and its application to the Bi-rich HgMn Star HR 7775*, *Astronomy & Astrophysics*, **388**, 692–703, 2002.
5. J. DUNNING, *NASA's electric propulsion program: Technology investments for the new millennium*, 37 AIAA/ASME/ASEE Joint Propulsion Conference, American Institute of Aeronautics and Astronautics, 2001, AIAA-2001-3224.
6. B. EDLÉN, *The refractive index of air*, *Metrologia*, **2**, 71–80, 1966.
7. D. GAWRON, S. MAZOUFFRE, C. BONIFACE, *A Fabry-Pérot spectroscopy study on ion flow features in a Hall effect thruster*, *Plasma Sources Science and Technology*, **15**, 4, 2006.
8. W.A. HARGUS JR., *Investigation of the Plasma Acceleration Mechanism within a Coaxial Hall Thruster*, Ph.D. Thesis, Leland Stanford Junior University, Stanford, CA 2001.
9. G. HERZBERG, *Atomic Spectra and Atomic Structure*, Dover Publications, New York 1994.
10. H.G. KUHN, F.R.S., *Atomic Spectra*, p. 194, Academic Press, New York 1969.
11. C. MARRESE-READING, A. SENGUPTA, R. FRISBEE, J. POLK, M. CAPPELLI, I. BOYD, M. KEIDAR, S. TVERDOKHLEBOV, S. SEMENKIN, T. MARKUSIC, A. YALIN, T. KNOWLES, *The VHTAL program to demonstrate the performance and lifetime of a bismuth-fueled very high I_{sp} Hall thruster*, 41st AIAA/ASME/SAE/ASEE Joint Propulsion Conference, American Institute of Aeronautics and Astronautics, 2005, AIAA-2005-4564.
12. N.B. MEEZAN, *Electron Transport in a Coaxial Hall Discharge*, Ph.D. Thesis, Leland Stanford Junior University, Stanford, CA 2002.
13. D.B. SCHARFE, M.A. CAPPELLI, *Stationary reference Bi discharge cell for optical diagnostics of a bismuth Hall thruster*, 29th International Electric Propulsion Conference, Electric Rocket Propulsion Society, 2005, IEPC-2005-058.
14. M.K. SCHARFE, C.A. THOMAS, D.B. SCHARFE, N. GASCON, M.A. CAPPELLI, *Shear-based model for electron transport in 2D hybrid Hall thruster simulations*, 43rd AIAA/ASME/SAE/ASEE Joint Propulsion Conference, American Institute of Aeronautics and Astronautics, 2007, AIAA-2007-5208.
15. M.K. SCHARFE, N. GASCON, M.A. CAPPELLI, E. FERNANDEZ, *Comparison of a hybrid Hall thruster model to experimental measurements*, *Physics of Plasmas*, **13**, 083505, 2006.
16. M.K. SCHARFE, C.A. THOMAS, D.B. SCHARFE, N. GASCON, M.A. CAPPELLI, E. FERNANDEZ, *Shear-based model for electron transport in hybrid Hall thruster simulations*, *IEEE Transactions on Plasma Science*, **36**, 5 (1), 2058–2068, 2008. The paper can be found online at: http://ieeexplore.ieee.org/xpls/abs_all.jsp?isnumber=4674691&arnumber=4663159&count=33&index=12.
17. I.I. SOBELMAN, *Atomic Spectra and Radiative Transitions*, second edition, p. 170, Springer-Verlag, New York 1992.
18. S. TVERDOKHLEBOV, A. SEMENKIN, J. POLK, *Bismuth propellant option for very high power TAL thruster*, 40th AIAA Aerospace Sciences Meeting & Exhibit, American Institute of Aeronautics and Astronautics, 2002, AIAA-2002-0348.

Received May 14, 2008.